Citation
Li, Z. and Chen, W. and Hao, H. 2018. Crushing behaviours of folded kirigami structure with square dome shape. International Journal of Impact Engineering. 115: pp. 94-105. http://doi.org/10.1016/j.ijimpeng.2018.01.013

Crushing behaviours of folded kirigami structure with square dome shape

Zhejian Li, Wensu Chen, Hong Hao*

Centre for Infrastructural Monitoring and Protection
School of Civil and Mechanical Engineering, Curtin University, Australia
Kent Street, Bentley, WA 6102, Australia

*corresponding author : hong.hao@curtin.edu.au

Abstract

In this study, a new type of aluminium sandwich structure with folded square dome as core is proposed. The square dome tessellated core is folded using a single piece of aluminium sheet. Four types of folded dome structures with different base sizes and top face configurations, i.e. 10 mm closed top dome, 20 mm closed top dome, 10 mm open top dome, 20 mm open top dome are studied. A single cube strip model is numerically simulated and calibrated with the experimental results from the previous studies. Good agreement on the peak and average stress between numerical results and test data is achieved. The calibrated model is then used to simulate structural response of the proposed folded dome shape structures. The damage modes and the structural responses including average and peak stress, energy absorption, uniformity ratio and densification strain are compared among these folded structures. The proposed square dome kirigami foldcore shows good energy absorption characteristics under quasi-static loading and dynamic loading by yielding a large densification strain, a low initial peak stress and a small ratio of average stress to peak stress. In addition, unlike the existing cube strip structures, the proposed folded square dome structure shows insensitivity to the crushing speed in terms of initial peak stress and uniformity ratio. Compared with the existing tessellated Kirigami foldcore of cube strip, the proposed folded square dome demonstrates a superior performance than most of Miura folded structures.

Keywords: square dome shape; kirigami; folded; flatwise crushing

1. Introduction

Sandwich structures have been extensively studied due to the lightweight and high energy absorption capacity [1]. The performances of sandwich structures with different cores under various loading conditions have been investigated. These cores includes conventional cores, such as metallic foams [2, 3], square and hexagonal honeycombs [4-6], trusses [7], lattices [8, 9], corrugated [10] and some recently proposed structural forms such as functionally graded [11, 12], multi-arched [13-15] and auxetic cores [16, 17].

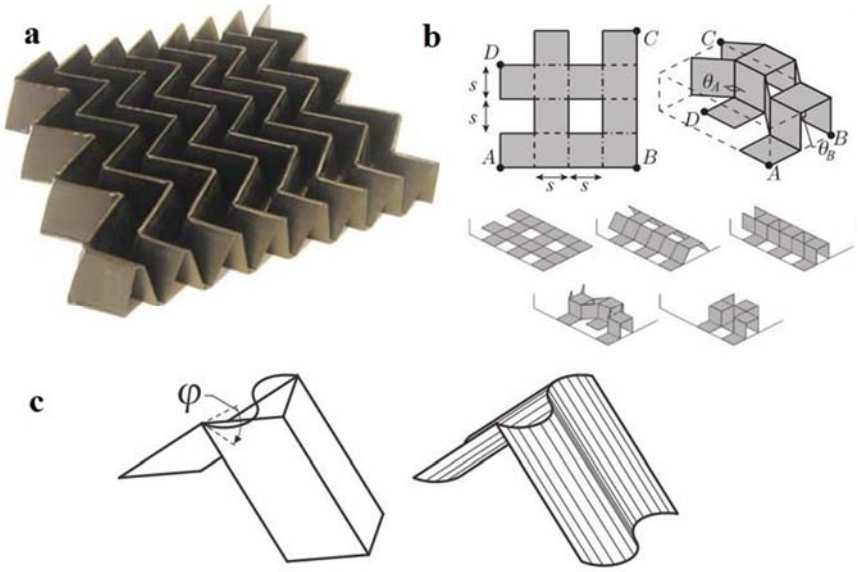

Figure 1. Typical foldcores (a) rigid foldable origami pattern or Miura-origami [18]; (b) rigid foldable kirigami pattern- cube foldcore [19]; (c) curved-crease origami pattern [20]

Folded core was proposed in 1972 by Miura [21] and has been intensively investigated recently. The folded core is acquired by folding sheet materials with origami patterns. Folded core can be categorized into three types: rigid foldable origami pattern, rigid foldable kirigami pattern and a variant of rigid foldable origami named curved-crease foldcores [19, 20, 22-24]. Examples of these three types of foldcores can be found in Figure 1. The rigid foldable origami pattern is made from an unbroken sheet folded along creases without stretching or twisting of

the panels. The rigid foldable kirigami pattern has the similar characteristics except that it is not folded from an unbroken sheet. The sheet may be cut, stamped or punched before folding. For the curved-crease foldcore, its creases are curved, which is different from the other two types where the creases are the combination of straight lines [19, 20, 22].

The Miura-origami foldcores have been investigated in detail. Miura foldcore is a type of rigid foldable origami pattern consisting of repeating tessellated shapes. A comprehensive review on Miura-origami foldcore was given by Heimbs [25]. Miura-type foldcore has the advantages such as continuous manufacture process and open ventilation channels which could address the issues of accumulation of humidity and heat when using conventional honeycomb as sandwich structure cores [26]. In terms of energy absorption or strength, the standard Miura-origami foldcore has inferior performance than a commercial honeycomb with comparable material and density [20]. The curved-crease foldcore was proposed and it had a higher energy-absorption capacity as compared with straight-crease foldcore or Miura-type, and slightly lower crushing resistance capacity than honeycombs in terms of average crushing stress [20]. However, the curved-crease foldcore has a more uniform failure response and a lower ratio of initial peak stress to average stress when compared with honeycomb structure.

As one of the proposed kirigami foldcores by Fathers et al [19], cube strip has a higher average stress comparing with original Miura-type foldcore and curved-crease foldcore. A 24% increase of average stress is demonstrated as compared to the previously studied best-performing curved-crease foldcore and a 74% increase of average stress is shown over the standard Miura-type foldcore under flatwise quasi-static crushing. However, cube strip is folded from several sheet strips instead of one sheet, the manufacturing could be a disadvantage comparing with the Miura-type foldcores which are folded from a single sheet.

In this study, a rigid kirigami foldcore with tessellated square dome is proposed. The proposed square dome pattern is inspired by a combination of bi-directional load-self-cancelling square dome structure and the kirigami patterns by Fathers et al [19]. Finite element analysis software LS-DYNA is employed in this study to analyse peak stress, average stress, energy absorption and densification strain of different foldcores. A numerical model of a foldcore with cube strip kirigami pattern under flatwise quasi-static crushing is firstly constructed and calibrated by comparing its generated stress-strain curves with the existing experimental data. The calibrated numerical model is then used to perform numerical simulations of the responses of the proposed foldcore structures. The proposed foldcores are compared with the cube strip kirigami structure, which has already demonstrated superior energy absorption capacity over other origami foldcores from the previous studies. In addition, various dynamic loading rates are applied on the proposed foldcores to investigate the effect of strain rate on structural response and energy absorption capacity of these foldcores.

2. Numerical Model Validation

In this study, finite element software LS-DYNA 971 is used for numerical simulation. Experimental data of the cube strip kirigami foldcore under quasi-static flatwise crushing by Fathers et al [19] is used for model calibration. The accuracy and reliability of the numerical model is examined by comparing the stress-strain curves. Folding configuration of kirigami cube strip foldcore is shown in Figure 2. Each row of cube strip is folded from a single strip of aluminium sheet and foldcore is then glued to the base plate. No connection or glue is placed between each row of cube strip. Each unit cell of cube strip foldcore consists of four 10 mm by 10 mm square faces and has a dimension of 20 mm by 10 mm by 10 mm in length, width and height, respectively. In the previous study, the strips are folded from aluminium 1100 alloy sheet with a thickness of 0.15 mm, which gives foldcore a volumetric density of ρ_v=3%.

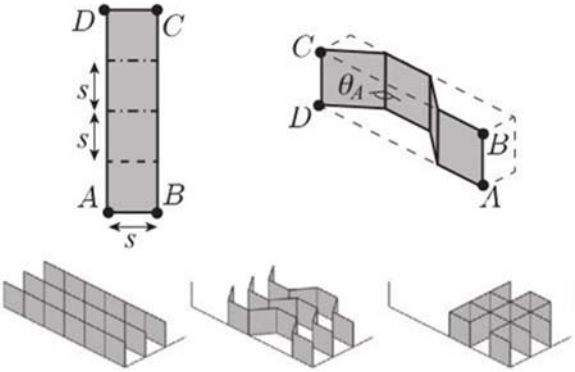

Figure 2. Crease pattern and folded configuration of kirigami foldcore with cube strip [19]

2.1. Numerical model

A numerical model is built with one folded unit cell as shown in Figure 3 (a). To verify the numerical model, it is similar to the numerical analysis in the previous study [19]. The foldcore unit cell is modelled by using default Belytschko-Tsay type shell element, as shown in Figure 3. An isotropic hardening material model *MAT_024 PIECEWISE LINEAR PLASTICITY is used for the material. The material properties and true plastic stress-strain data for the sample material are listed in Table 1 and Table 2, respectively. The unit cell is fixed onto a rigid plate by constraining the bottom edges of the cell. The sample is then flatwise crushed till around strain ε=0.8 by another rigid plate from top with a constant crushing speed of 0.05 m/s. It should be noted that computational cost for explicit simulation by using experimental quasi-static loading speed (1mm/min) is too expensive, in this study the crushing speed of 0.05 m/s is adopted because it was found sufficient to ensure quasi-static conditions in the simulation [19]. Top rigid crushing plate is set to have only one-degree of freedom in vertical direction, which simulates flatwise crushing experiment. The self-contact of the foldcore is modelled by the keyword *CONTACT AUTOMATIC SINGLE SURFACE. The contacts between foldcore and top/bottom plates are modelled by *CONTACT AUTOMATIC NODES TO SURFACE. Friction coefficient of 0.25 is used for the contact interactions. Figure 3 (b/c/d/e) show the

numerical models of the proposed unit cells, together with the folded unit cell shown in Figure 3 (a) used for model validation.

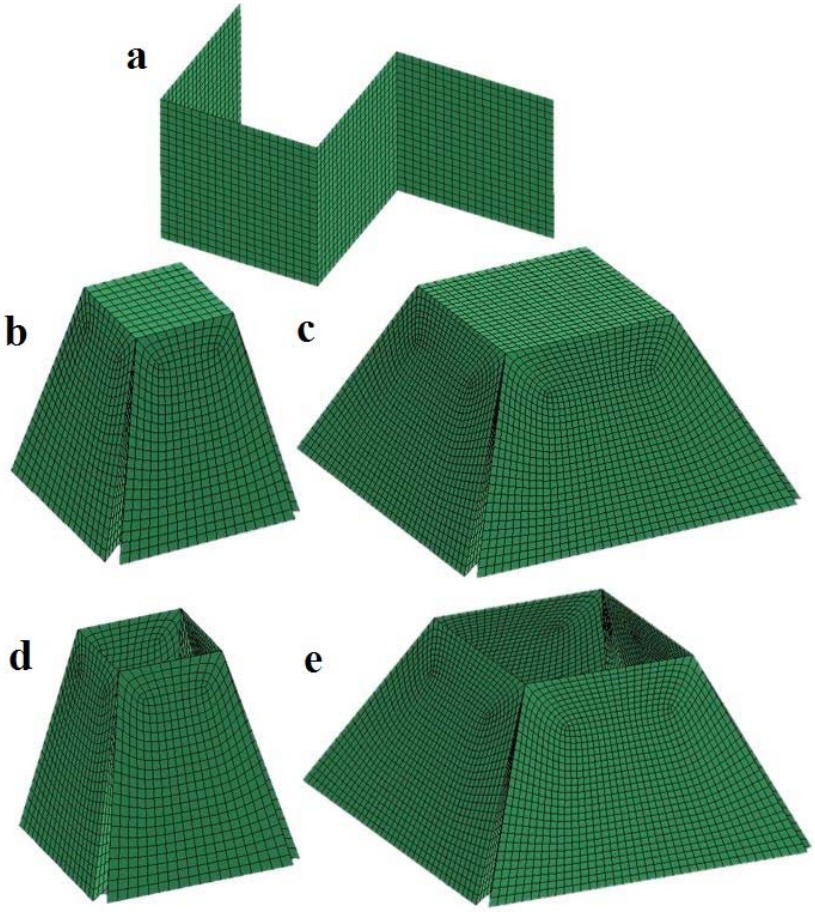

Figure 3. Single unit cell with mesh size of 0.5 mm, (a) kirigami cube strip foldcore, (b) 10 mm closed top square dome foldcore, (c) 20 mm closed top square dome foldcore, (d) 10 mm open top square dome foldcore, (e) 20 mm open top square dome foldcore

Parameter	**Young's modulus (GPa)**	**Poisson's ratio**	**Yield stress (MPa)**	**Density (kg/m^3)**
Value	69	0.33	23.9	2710

Table 1. Material properties of Aluminium 1100 alloy [27]

Strain	0	0.007	0.019	0.048	0.106	0.183	0.260
Stress (MPa)	23.9	38.4	51.9	67.8	83.6	96.1	105.8

Table 2. True plastic stress-strain data of Aluminium 1100 alloy from experiment *[19]*

2.2. Mesh convergence test

As an important factor for determining both the computational cost and simulation accuracy, mesh size convergence tests are carried out with four element sizes of 1 mm, 0.5 mm, 0.25 mm and 0.125 mm. Stress is calculated from the reaction force of crushing a foldcore unit cell and its base area, i.e., 10 mm by 20 mm for cube strip foldcore. As shown in Figure 5 (b), the top edges of each unit cell of the tested foldcore are not all on the exact same elevated level, due to manufacturing error. The 0.5 mm manufacturing imperfection, which is equal to 5% strain for this 10 mm high foldcore, was considered in the numerical simulations conducted by Fathers et al [19]. However, the imperfection is removed to simplify the simulation in the mesh convergence tests of this study. The average stress of a unit cell is calculated using base area of 20 mm by 10 mm. The results of the mesh convergence test are shown in Figure 4.

As shown in Figure 4, no obvious difference in the peak stress and the flowing stress obtained with these four different mesh sizes. However, mesh size has significant effect on the densification stage. Numerical result of using 1 mm mesh yields a much smaller densification strain and higher stress. The other three mesh sizes (0.5 mm, 0.25 mm, 0.125 mm) generate similar results and a good agreement is obtained comparing with the experimental and numerical data given in [19]. Therefore, 0.5 mm mesh size is used in the subsequent simulations.

It is noted that the initial stiffness, i.e., the slope before the initial peak stress corresponding to the experimental data in [19] is smaller than the numerical result. This is caused by the variation of core height of the sample induced by the folding process in preparing the testing samples as mentioned above. Other than that, the comparison demonstrates the numerical model yields good predictions of the performance of a foldcore. It should be noted that the initial imperfection of the foldcore, which is probably inevitable in practice, is not considered in the

present analysis since it does not affect the performance of the foldcore in terms of the initial peak stress, plastic flow and densification process.

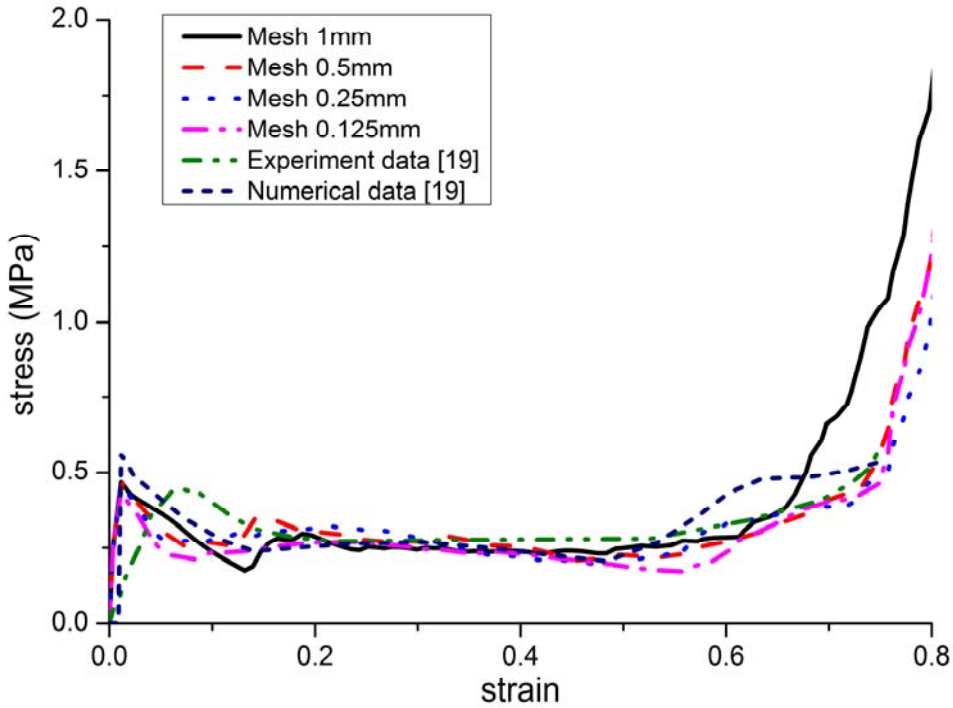

Figure 4. Stress-strain curves of cube strip foldcore with different mesh sizes and comparison with the experimental and numerical data in [19]

3. Geometries of Folded Square Dome Core

The traditional kirigami folded cube pattern [28] and kirigami cube strip pattern [19] previously studied have one drawback. Adjacent vertical faces of each unit cell of the foldcore are not constrained, that is no vertical constraint or connection exists between each row of folded cube strip and vertical constrain or connection does not exist on all vertical faces of folded cube pattern. Folding process of cube pattern is shown in Figure 1 (b), and some of the obvious loose edges for both foldcores are marked out in red shown in Figure 5. This might be one of the main causes for the inferiority of cube strip foldcore as compared to the square honeycomb with the same unit cell configuration in terms of crushing resistance.

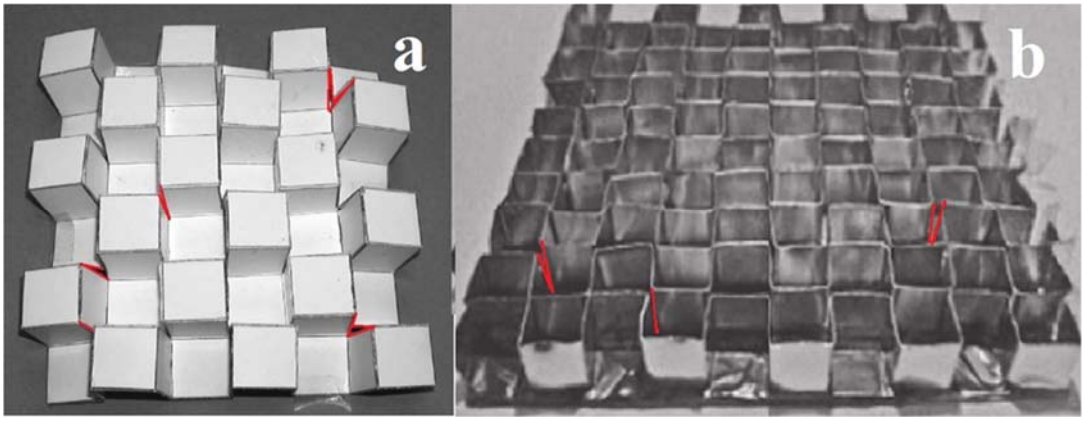

Figure 5. Unconstrained adjacent vertical faces (a) cube foldcore [28] (b) cube strip foldcore [19]

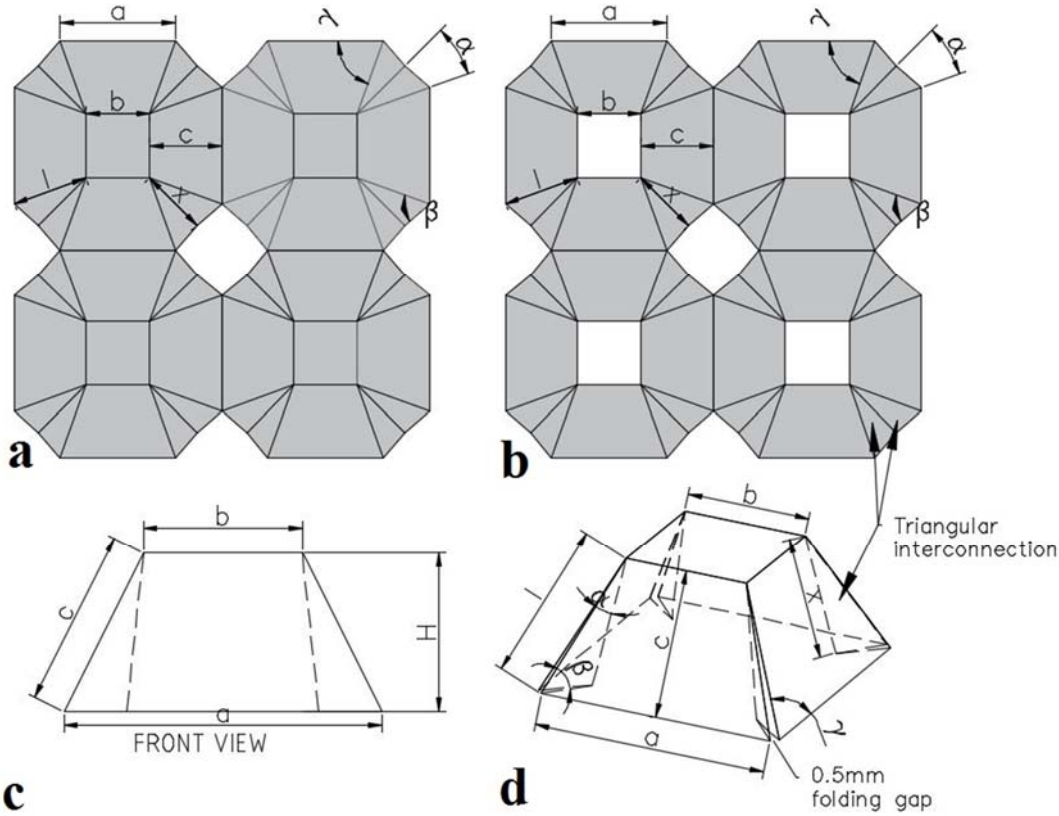

Figure 6. (a) Crease pattern of closed top square dome foldcore; (b) Crease pattern of open-top square dome foldcore; (c) front view of a unit cell of square dome foldcore; (d) isometric view of folding configurations of square dome foldcore

To improve the performance, the adjacent faces on square dome of the proposed foldcores are designed to be connected. This is achieved by adding triangular interconnections between two

adjacent sidewalls of the folded core, as shown in Figure 6 (b) (d). These interconnections provide extra supports for out-of-plane loading. To properly represent the near-fully-folded configuration in reality, slight gap of 0.5 mm is assumed in the numerical models, also shown in Figure 6 (d). The folding creases are marked in continuous line in Figure 6 (a). The only cut-out requirement for folding is the octagon shape in the centre of four adjacent unit cells. For the structure with open top, the smaller squares in the centre of each unit cell are cut out and then the sheet is folded in the same way as the square dome with closed top.

The added sidewall interconnections constrain the dimension of the foldcore. The top angle of triangular interconnection i.e. alpha α, is restricted by the top and base square length, *a*, *b*, and the height of the square dome, *H* as shown Figure 6 (c). The volumetric density ρ_v, is kept constant as 3% throughout this study. Accordingly, the thickness of the foldcore *t* is modified based on the calculated surface areas of each core. For the proposed square dome foldcore, the shape of the unit cell and the interconnections of sidewalls are determined by three parameters, i.e. *a, b, H*. Other geometry parameters shown in Figure 6 can be determined by these three parameters as follows:

$$c = \sqrt{\frac{(a-b)^2}{2} + H^2}\ ;\ l = \sqrt{\frac{(a-b)^2}{2} + c^2}\ ;\ \gamma = arctan\ (\frac{2c}{a-b})\ ;\ \alpha = \gamma - \frac{\pi}{4}\ ;$$

$$\beta = arcos(\frac{\sqrt{2}a - \sqrt{2}b}{2l})\ ;\ x = \frac{sin\beta \cdot l}{\sin\ (\pi - \alpha - \beta)}\ ;$$

The total surface area for each closed top unit cell $A = b^2 + 4 * \frac{1}{2}c(a+b) + 8 * \frac{1}{2}\sin\alpha \cdot xl$;

The total surface area for each open-top unit cell $= 4 * \frac{1}{2}c(a+b) + 8 * \frac{1}{2}\sin\alpha \cdot xl$;

The relative density, or volumetric density, $\rho_v = \frac{A \cdot t}{a^2 H}$.

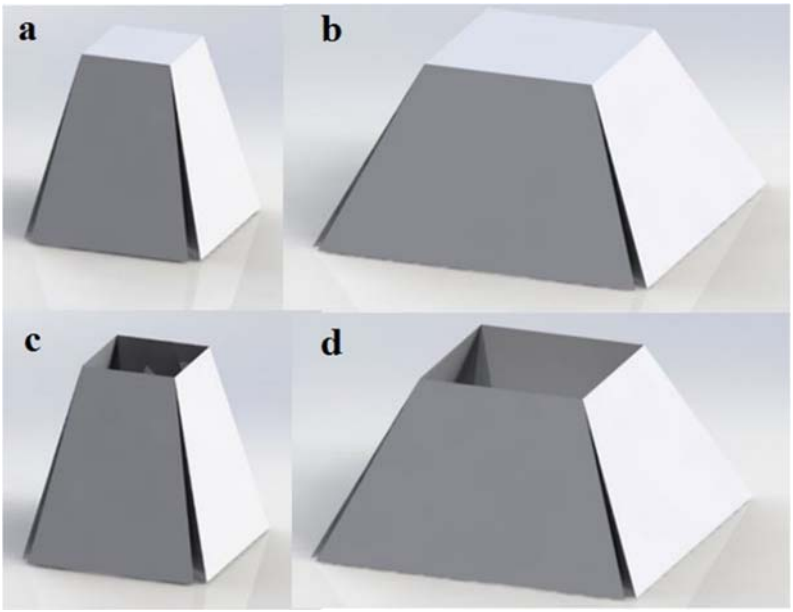

Figure 7. Four configurations of folded square dome, (a) D10-CT; (b) D20-CT; (c) D10-OT; (d) D20-OT

Two types of kirigami foldcores with square dome, each with two different base dimensions are investigated in this study. One type of foldcore is square dome with top face and another type is the same square dome but without top face. The top face of each dome can be removed as it provides little contribution to energy absorption in flatwise crushing of the foldcore. Height, H, is set as 10 mm for all the four square dome foldcores. For the 10 mm closed top square dome foldcore, $a=10$ *mm,* $b=5$ *mm* and $t=0.055$ *mm* to achieve a 3% relative volumetric density. For the 10 mm open-top square dome foldcore, t is calculated to be 0.057 mm. For the square dome foldcore with the base size of 20 mm, the thickness of the wall is calculated to be 0.13 mm and 0.147 mm, for the closed and open top foldcores, respectively. These foldcores are denoted as D10-CT, D10-OT, D20-CT, D20-OT, which define the base length a (10 mm or 20 mm) and the closed or open top on the foldcores. The illustrations of four configurations of foldcores are shown in Figure 7.

4. Quasi-static Flatwise Crushing

Structural responses of quasi-static flatwise crushing of four types of foldcores are obtained from numerical simulations and compared with the calibrated cube strip foldcore. Average plateau stress, σ_{ave}, densification strain, ε_D, and peak stress, σ_{peak}, are used for analysis and evaluation of the foldcores. The stress-strain curves are calculated from the force-time (*P*-*T*) curves obtained from the numerical simulations, where the vertical reaction forces are exerted on the rigid crushing plate under a constant speed (v). Stress, σ, is equal to the reaction force divided by the base area instead of top area, given as $\sigma = \frac{P}{a^2}$, since the stress calculated from base area can better describe the force and stress transmitted to the protected structure and the energy absorption capacity of the folded core. Strain is calculated using the product of time and crushing speed divided by the overall height of the foldcore, given as $\varepsilon = \frac{vT}{H}$, where T is the time since the beginning of crushing.

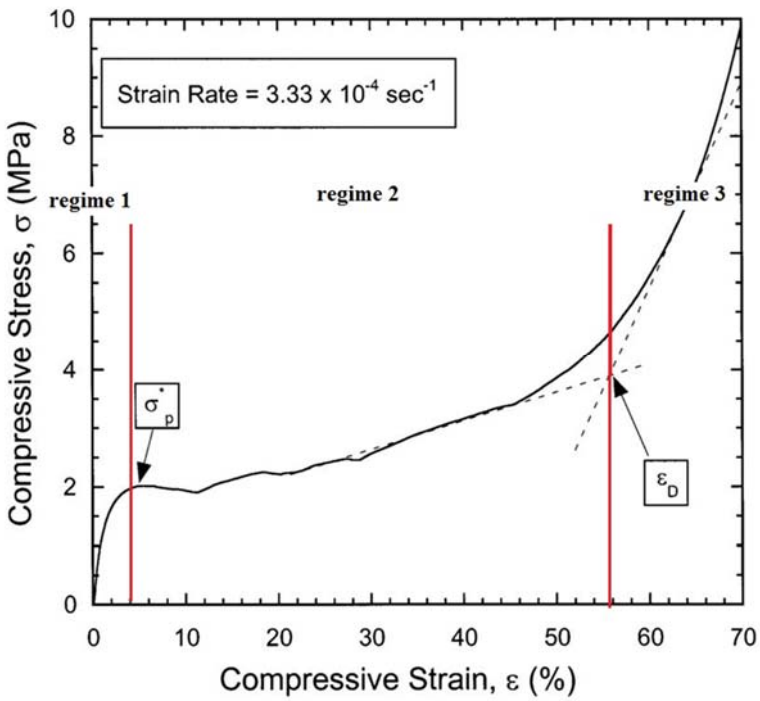

Figure 8. Example of stress-strain curve of a typical aluminium foam under quasi-static crushing with three regimes and the illustration of densification strain [29]

The behaviour of all foldcores under quasi-static crushing, as shown in Figure 9, are similar to that of the aluminium foam [29-31]. As shown in Figure 8, three regimes are present for a typical stress-strain curve of aluminium foam under quasi-static crushing. They are: 1) Linear elastic regime at low stresses; 2) Long plateau regime where localized plastic collapse propagates through foldcore; and 3) Densified regime that structure is fully collapsed with a rapid rise in stress with further strain.

Similar to aluminium foam, the densification strain (ε_D) calculated in this study is defined by the intersection of two asymptotic curves of the stress-strain response at plateau and densified regimes, as illustrated in Figure 8. The average plateau stress is the internal energy absorption before densification divided by densification strain, and it is calculated as $\sigma_{ave} = \frac{\int_0^{\varepsilon_D} \sigma(\varepsilon)\cdot d\varepsilon}{\varepsilon_D}$.

Since the initial peak stress of square dome foldcores is much lower than its average stress, σ_{peak} is defined herein by the peak value of stress in plateau regime as marked in Figure 9. The uniformity ratio U between peak stress and average stress acts as an indicator of the uniformity of energy absorption.

4.1. Stress-strain curve comparison among five foldcores

Stress-strain curves of different foldcores are presented in Figure 9. D20-OT demonstrates the best performance among these foldcores, with a very low initial peak stress, a high plateau stress and a good densification strain. Similar significant reduction of initial peak stress at the end of linear elastic regime can be observed when comparing other three proposed square dome foldcores with cube strip. Although these three square dome foldcores, i.e. D10-CT, D10-OT and D20-CT, have a slightly decrease in plateau stress and densification strain than cube strip foldcore. The occurrence of the overall peak stress is also delayed for all square dome foldcores to strain at about 0.1 to 0.3 at the plateau regime instead of initial linear elastic regime as cube strip foldcore. When comparing the open-top square domes i.e. D20-OT, D10-OT to their

same-sized square domes with closed top i.e. D20-CT and D10-CT, a noticeable rise in plateau stress and slight increase in densification strain can be observed. It is because the closed top square domes have a thinner wall thickness than their same-sized open top foldcores but the top face provides little resistance against quasi-static flatwise crushing of the foldcore.

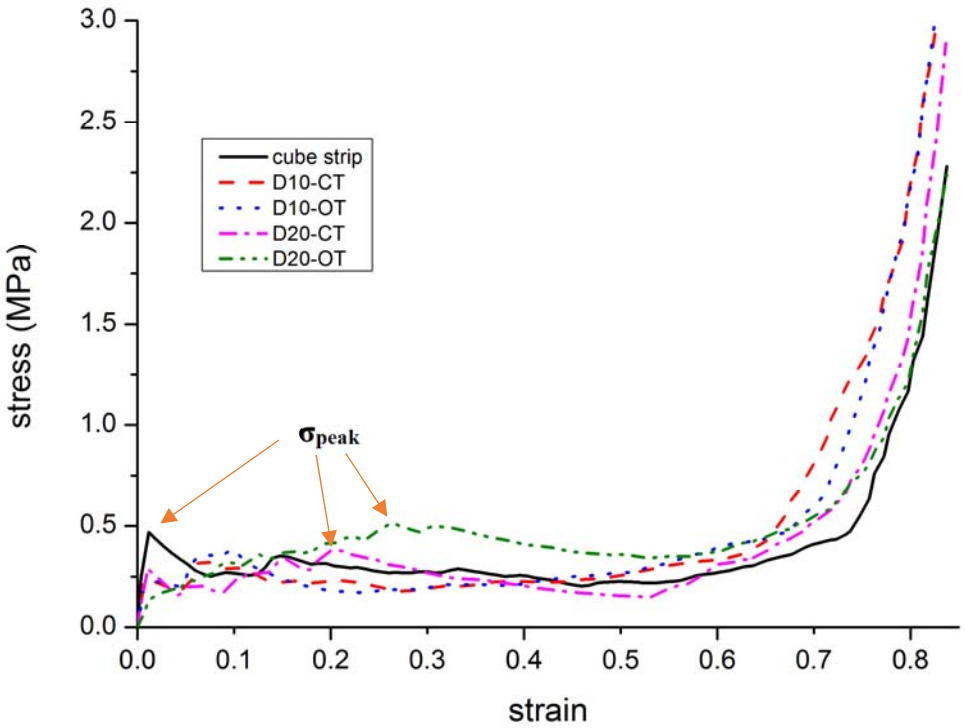

Figure 9. Stress-strain curves of five foldcores under quasi-static flatwise crushing

The average stress, peak stress, densification strain and uniformity ratio are listed in Table 3. Comparing the plateau stress before densification, cube strip foldcore and three square dome foldcores i.e. D10-OT, D10-CT and D20-CT, have similar value. D20-OT holds the highest average plateau stress at 0.389 MPa, around 36% higher than the second highest average plateau stress of the cube strip foldcore of 0.286MPa. D10-OT, D10-CT and D20-CT have similar peak stress around 0.35 MPa. Densification strains of these foldcores are similar in value, around 0.7 except for D10-CT. For an ideal energy absorption material or structure, the following characteristics are expected: low initial peak stress, high densification strain and a high plateau stress. As can be observed from Table 3, D20-OT has a low uniformity ratio, high

plateau stress and densification strain. It can be concluded that D20-OT has the best performance with regards to energy absorption capacity among these five foldcores.

Parameter	Cube strip	D10-CT	D10-OT	D20-CT	D20-OT
σ_{peak} (MPa)	0.469	0.325	0.375	0.384	0.508
σ_{ave} (MPa)	0.286	0.250	0.275	0.264	0.389
ε_D	0.72	0.65	0.69	0.71	0.72
$U= \sigma_{peak} / \sigma_{ave}$	1.64	1.30	1.36	1.46	1.31

Table 3. Average plateau stress, peak stress, densification and ratio U of five configurations of foldcores under flatwise quasi-static crushing

As given in Table 3, although the average stresses of plateau stage of D10-CT, D10-OT and D20-CT are slightly lower than that of the cube strip, their uniformity ratios are significantly improved. Furthermore, a delay of peak stress can be easily noticed from the stress-strain curves of these three square dome foldcores, which indicates that it is easier to deform at the early stage for the proposed square dome foldcores. D20-OT outperforms the other three square dome foldcores and the cube strip in all four key indicators, indicating it is the best design among those considered in the study for potential application of kirigami square dome foldcore in terms of energy absorption.

4.2. Damage mode of the foldcores

The damage modes of the square dome foldcores are different from the cube strip foldcore. Damage modes are shown in Figure 10 with flatwise crushed foldcores at the strains of 0.2, 0.4 and 0.6, respectively. Similar to widely investigated square honeycomb structures [4, 32, 33], cube strip foldcore can be treated as square honeycomb without connections between adjacent rows. The deformation mode for cube strip foldcore is governed by buckling and followed by sequential folding of the core sidewalls. Less constraint between adjacent unit cells of cube strip results in an easier buckling behaviour at initial crushing than square honeycomb structures. The square dome foldcores yield different collapse patterns. At initial stage of the

crushing, the side walls of square dome foldcore are prone to bend and roll inwards towards the centre of unit cell. This is because the sidewalls are leaning towards the centre, which is different from the vertical sidewall of the cube strip foldcore or square honeycomb structures. Once the rigid plate is in contact with the foldcore, the inclined sidewalls bend under the vertical load. Due to the inward bending of the top edges of sidewalls, the top surface of the folded domes, D10-CT, D20-CT becomes a dent instead of a flat surface, as can be seen in Figure 10.

This action of bending and rolling stops with further crushing, as there are two triangular interconnections at each corner for the square dome foldcores, providing increased resistance against bending and rolling. Because of the triangular geometries of the interconnections, with increasing cross-section area from top to bottom, the crushing resistance increases with the crushing deformation. This can be confirmed by comparing damage mode of D10-CT with D20-CT and comparing D10-OT with D20-OT as shown in Figure 10. Due to the smaller size of triangular interconnections which are determined by the unit cell parameter *a, b* and *H*, the bending of the sidewalls towards centre for D20-CT is more severe than D10-CT at the strain of 0.2. Similarly, more bending deformation at the top edge of the sidewall for D20-OT can be observed than D10-OT at the same strain. It is because D20-OT has a smaller interconnection at each corner of the cell. Another reason is that D20-OT has a more inclined sidewall toward centre of each unit cell than D10-OT, thus making the sidewalls of D20-OT easier to bend and roll inward.

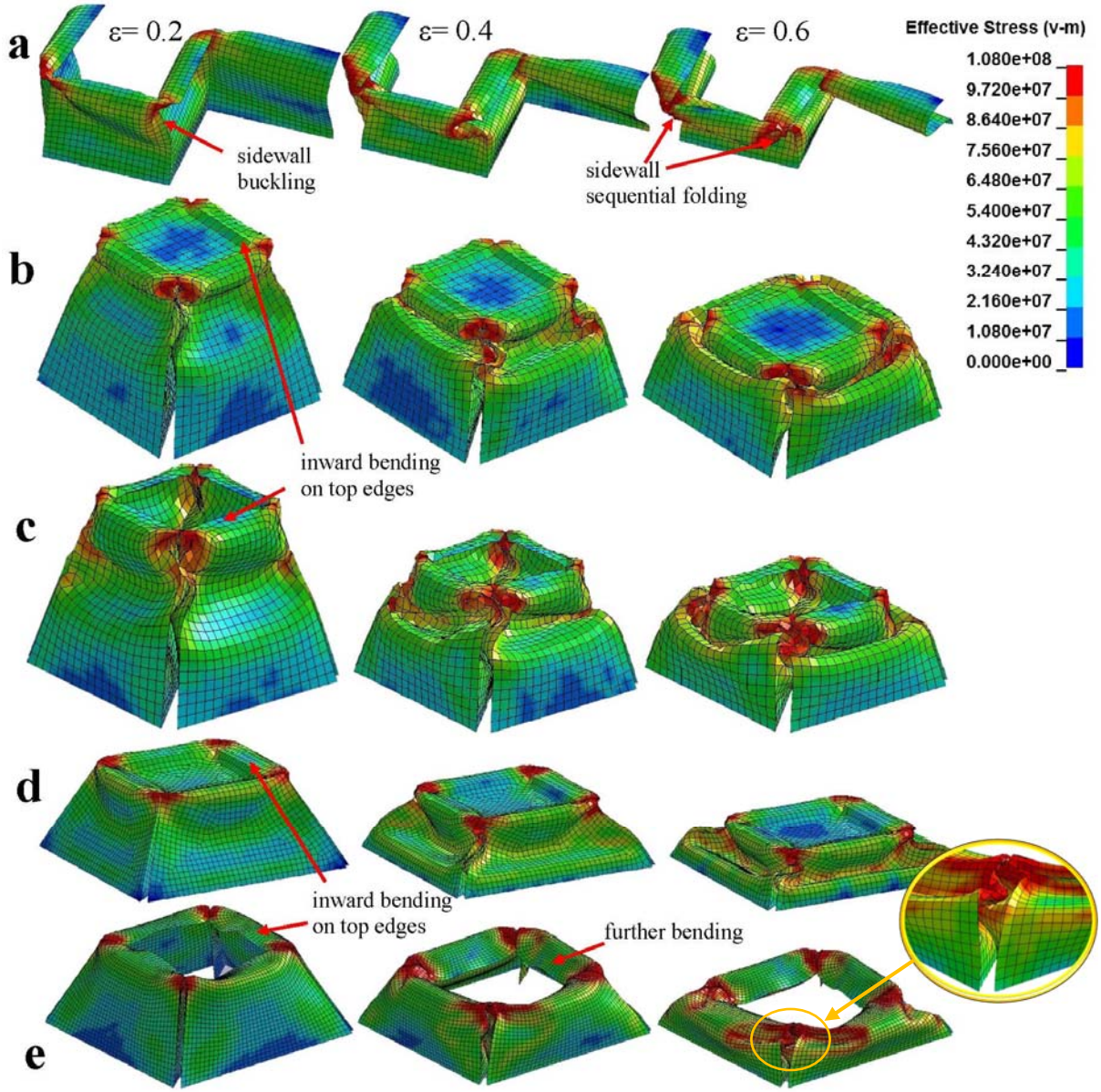

Figure 10. Damage modes of five foldcores at the strain of 0.2, 0.4 and 0.6 under quasi-static crushing of 0.05 m/s, a) cube strip; b) D10-CT; c) D10-OT; d) D20-CT; e) D20-OT (Note: D20-CT and D20-OT are scaled down to fit into one graph)

The damage of the foldcore can be reflected from the stress-strain curves. The peak stress of the plateau regime represents the end of the top edge sidewall bending deformation towards the centre. As shown in Figure 9, peak stress occurs before or around the strain of 0.2 for D10-CT, D10-OT, D20-CT foldcores and D20-OT foldcore has peak stress around the strain of 0.3. In Figure 10 (b-d), there are no further bending of sidewalls at top edges from the strain of 0.2 to 0.4 for D10-CT, D10-OT and D20-CT. In Figure 10 (e), further bending deformation of

D20-OT can be found when comparing the deformation at the strain of 0.2 and 0.4. As observed in Figure 11, crushing stress of D20-OT increases from the strain of 0.2 to 0.3 and reaches the peak value at the strain around 0.3, where bending deformation stops and sidewall buckling initiates. After the strain of 0.3, the damage of foldcore is dominated by the buckling of the sidewall only without any further bending of the top edges.

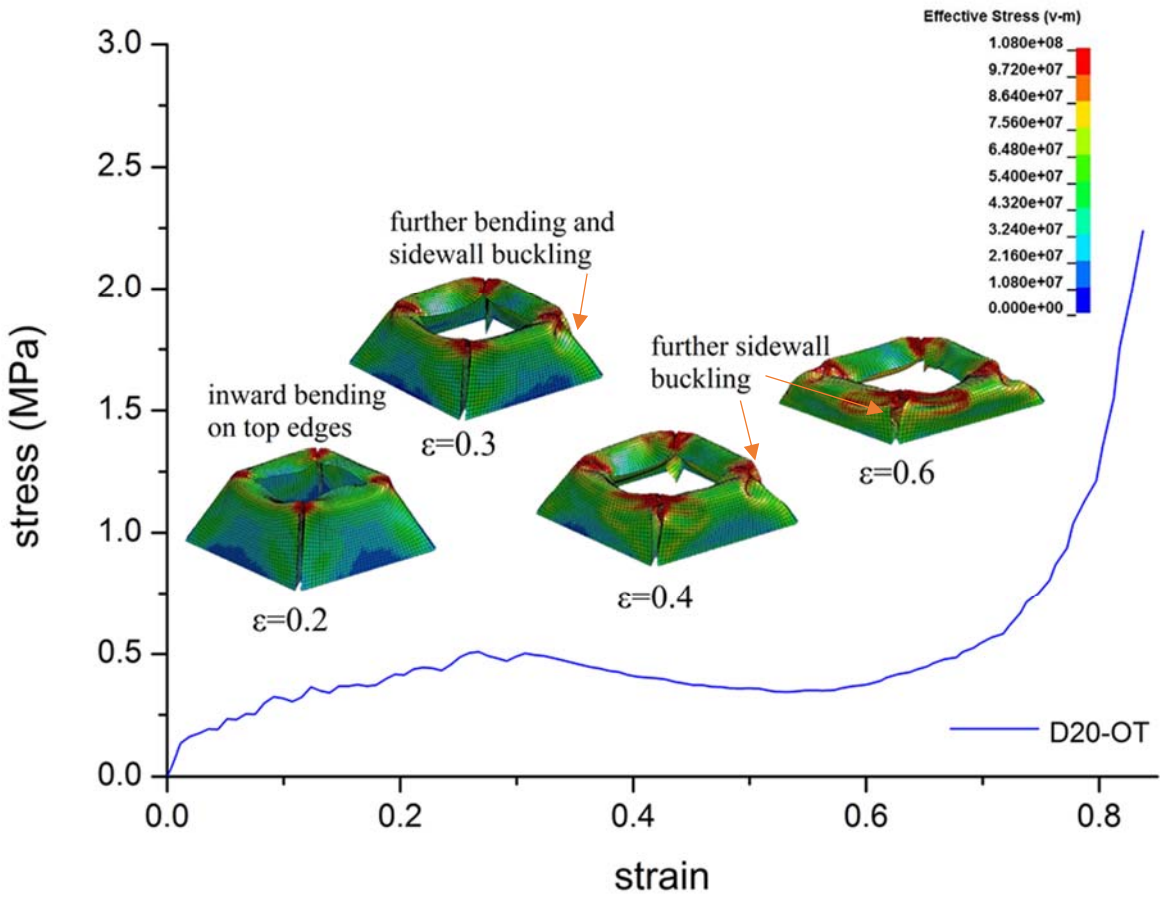

Figure 11. Stress-strain curve and damage mode of foldcore D20-OT at the strain of 0.2, 0.3, 0.4 and 0.6

This correlation between peak stress and buckling initiation indicates the occurrence of peak stress is associated with the bending deformation on sidewall top edges and the resistance of the interconnections. Smaller size of the triangular interconnections leads to lower resistance against bending of top edge of sidewalls and a delayed occurrence of peak stress. Once the bending deformation on top edges of sidewalls stops, typical buckling deformation of the cell

walls is then followed along with multi-folding of the interconnections. Buckling of the interconnections are circled and enlarged in Figure 10.

5. Dynamic Flatwise Crushing

5.1. Stress-strain curves under various crushing velocities

In this section, the foldcores are studied under different loading rates of crushing i.e. 0.05 m/s, 0.25 m/s, 0.5 m/s, 2.5m/s, 12.5 m/s and 25 m/s. The quasi-static crushing speed of 0.05 m/s is used as a baseline to evaluate the performance. The same parameters as quasi-static crushing are used in the dynamic crushing scenario analyses. Stress-strain curves of foldcores under various loading rates are shown in Figure 12. Average stress, peak stress, densification strain and uniformity ratio are given in Table 4.

It is found that loading rate has only slight effect on the densification strain of cube strip foldcore. However, the initial peak stress is greatly affected by the increase of loading rate for cube strip foldcore. The initial peak stress increases by 362% from 0.469 MPa to 2.165 MPa with the loading rate increasing from 0.05 m/s to 25 m/s as shown in Table 4 and Figure 12 (a), indicating great loading rate sensitivity of the structure. It should be noted that the strain rate effect on aluminium material properties are not considered in the present numerical study. Therefore, the observed increase in the initial peak stress is a loading rate effect on the structure, which as shown in Figure 12 is structural form dependent. The peak stress of the square dome foldcores is less influenced by the increasing in crushing speed, especially for the foldcores with open top. For the two foldcores with closed top, i.e. D10-CT and D20-CT, a significant increase in the initial peak stress due to the top face is also observed. However, the crushing resistance in plateau regime is less affected comparing with cube strip foldcore. For the two square dome foldcores with open top, i.e. D10-OT and D20-OT, their initial peak stress are barely effected at low crushing speed below 2.5 m/s as shown in Figure 12(c), (e). When the

crushing velocity is 12.5m/s and 25.0m/s, the initial peak stress of the two square dome foldcores with open top also increases, but at a smaller rate as compared to the other three foldcores considered in the study. The increase of the initial peak stress of the D20-OT is insignificant with the crushing velocity, indicating it is insensitive to the loading rate. These observations demonstrate that square dome foldcores with open top outperform the cube strip foldcore and the square dome foldcores with closed top, and due to the less sidewall constraints, smaller inclining angle of sidewalls and smaller interconnections, D20-OT has a better performance under dynamic loading conditions than D10-OT. Dynamic effects on this proposed structure are discussed in the following section.

Type	Crushing speed	σ_{peak} (MPa)	σ_{ave} (MPa)	ε_D	U= σ_{peak} /σ_{ave}
Cube strip	**0.05 m/s**	0.469	0.286	0.72	1.64
	0.25 m/s	0.460	0.326	0.71	1.41
	0.5 m/s	0.690	0.339	0.71	2.04
	2.5 m/s	1.195	0.426	0.69	2.81
	12.5 m/s	1.940	0.627	0.69	3.09
	25 m/s	2.165	0.939	0.62	2.31
D10-CT	**0.05 m/s**	0.325	0.250	0.65	1.30
	0.25 m/s	0.338	0.247	0.65	1.37
	0.5 m/s	0.355	0.246	0.66	1.44
	2.5 m/s	0.408	0.273	0.67	1.50
	12.5 m/s	0.666	0.382	0.70	1.74
	25 m/s	1.180	0.485	0.72	2.43
D10-OT	**0.05 m/s**	0.375	0.275	0.69	1.36
	0.25 m/s	0.398	0.295	0.68	1.35
	0.5 m/s	0.373	0.276	0.69	1.35
	2.5 m/s	0.493	0.280	0.69	1.76
	12.5 m/s	0.610	0.369	0.69	1.65
	25 m/s	0.730	0.442	0.66	1.65
D20-CT	**0.05 m/s**	0.384	0.263	0.71	1.46
	0.25 m/s	0.359	0.256	0.71	1.40
	0.5 m/s	0.346	0.247	0.70	1.40
	2.5 m/s	0.494	0.228	0.69	2.16
	12.5 m/s	0.644	0.293	0.69	2.20
	25 m/s	1.494	0.355	0.71	4.20
D20-OT	**0.05 m/s**	0.508	0.389	0.72	1.31
	0.25 m/s	0.504	0.381	0.72	1.32
	0.5 m/s	0.519	0.377	0.72	1.38
	2.5 m/s	0.529	0.381	0.73	1.39
	12.5 m/s	0.559	0.393	0.69	1.40
	25 m/s	0.694	0.413	0.67	1.68

Table 4. Average stress, peak stress, densification strain ε_D and uniformity ratio U of foldcores under various loading rates.

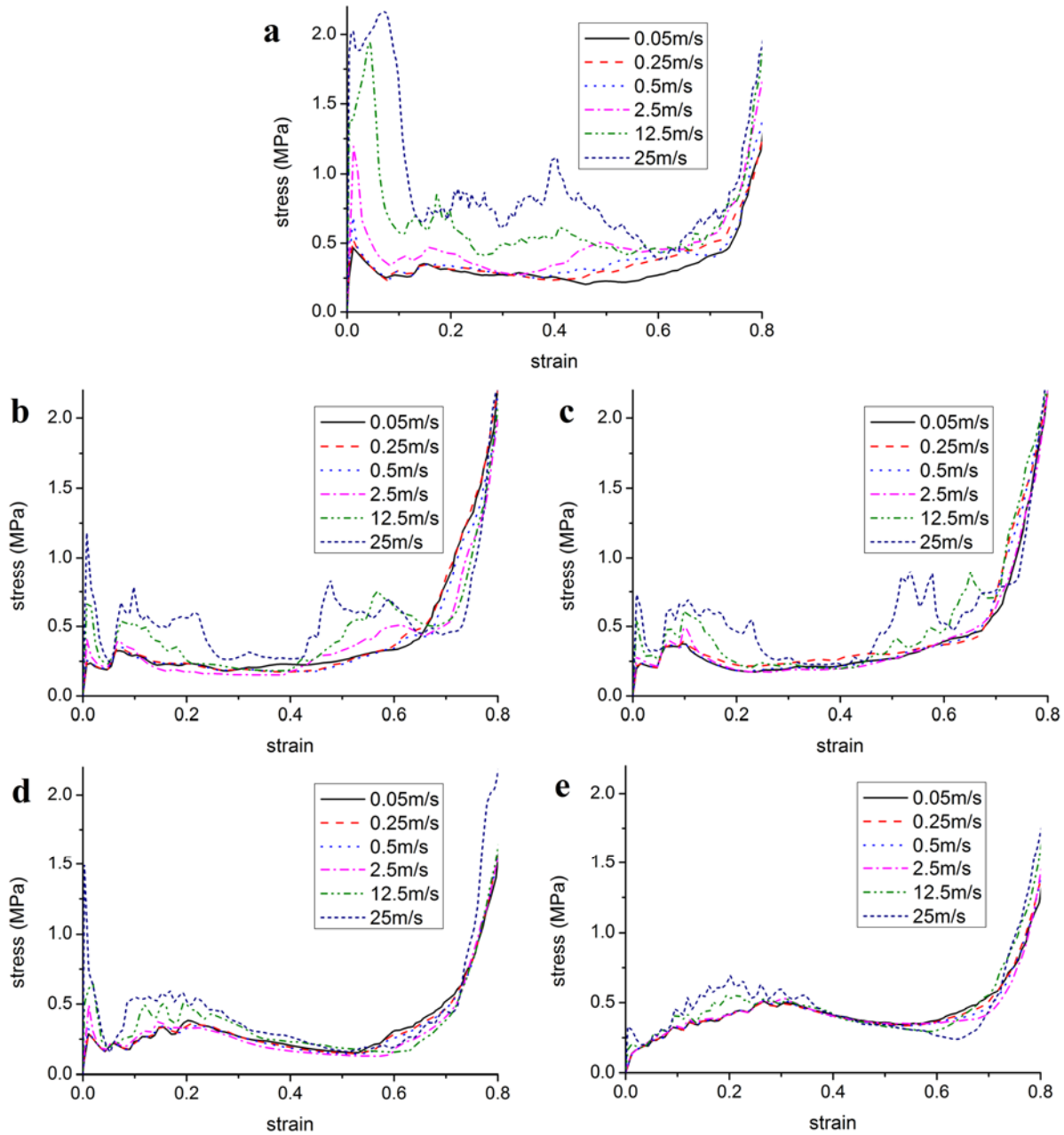

Figure 12. Stress-strain curves of five foldcores under different loading rate, a) cube strip; b) D10-CT; c) D10-OT; d) D20-CT; e) D20-OT

Although a sharp rise of initial peak stress can be observed for closed top square dome foldcore at high crushing rate, the average plateau stress of both closed and open top square dome

foldcores demonstrate superior insensitivity than cube strip foldcore. Insensitivity of uniformity ratio to loading rate is observed for the open-top square dome foldcores. In a previous study [34], it was reported that the plateau stress of aluminium foam was dependent on the relative density of the core by a power law and it was not sensitive to strain rate under low or medium loading rate. This strain rate insensitivity of plateau stress of square dome foldcore is similar to that of aluminium foam. Therefore, the square dome foldcore can be a potential replacement of aluminium foam core. In addition, foldcore can be cheaper, easier to manufacture and customized to fit different purposes.

5.2. Dynamic effects of the foldcores

Three dynamic effects: i.e. inertial resistance, inertial stabilization of cell walls against buckling and material strain-rate dependence were identified by Xue and Hutchinson in their study of square honeycomb sandwich cores [4]. As aluminium material shows less strain rate effect [35], the strain rate effect of material is not considered in the numerical material model. The dynamic effects on cube strip and square dome foldcores are only determined by structural forms rather than material itself. As mentioned earlier, cube strip foldcore has the similar geometry as square honeycomb, except that each row of unit cells is separated along vertical edges. Therefore, beside the inertial resistance of the sidewalls, the perpendicular cell walls delay the onset of wall buckling and maintain the strength of the core under dynamic loading due to the inertial stabilization of the sidewalls, which is similar to dynamic effect of square honeycomb structures. Hence, great rise of reaction force is expected for cube strip foldcore at initial stage with the increase of crushing loading rate, as shown in Figure 12 (a). Similar stress-strain response can be found in dynamic response of square honeycomb structure [4].

For the square dome foldcores, the deformation mode is different. At the early stage of the crushing, the vertical wall experiences no buckling and the top edges of sidewalls undergo bending deformation. Then the buckling deformation of the sidewall is followed. For square

dome foldcores with closed top, the square top face can act similarly as cell wall of honeycomb structure, to resist the bending deformation of top edges on sidewalls and stabilize the adjacent sidewalls during dynamic loading. Secondly, as the flat top face is parallel to the crushing plate, impact time is extremely short and inertial resistance increase dramatically with loading rate. Consequently, the closed top foldcores, i.e. D10-CT, D20-CT are more sensitive to loading rate in terms of initial peak than the open-top square dome foldcores, i.e. D10-OT, D20-OT. Moreover, as shown in Figure 12 after the initial contact between top face and the crushing plate, the crushing resistance of closed top square dome foldcores are less influenced by the loading rate as compared to the cube strip foldcore.

The inclining angle of sidewalls, size of the unit cell and triangular interconnections affect the crushing resistance of the structure under dynamic loading. With a higher inclining angle, the sidewalls of D10-OT are more vertical and it has a higher initial peak stress than the less inclined D20-OT especially under high loading rate. Similar result has been obtained by comparing honeycomb structure with perfectly vertical cell walls and pre-bend cell walls [4]. The initial peak of the foldcore is also related with the aspect ratio of the unit cell which is defined as the height over the size of the cell. Under the same height, smaller cell size leads to a higher constrain factor, therefore, a higher initial peak stress [36]. In other word, foldcore with smaller unit cell has more sidewall constraints per unit area, which leads to a stronger stabilization effect under high loading rate. However, under the same relative density, cell thickness is depended on the size of the unit cell as well. Increase in size of unit cell reduces the constraints per unit area but increases the thickness of the cell and may lead to an overall increase in initial peak stress. The larger size of vertical triangular interconnections also increases the initial crushing resistance under high loading rate. To conclude, due to the larger size of the interconnections, D10-OT with smaller cell size and higher inclining angle of sidewalls is more sensitive to the loading rate than D20-OT, as shown in Figure 12 (c) (e).

5.3. Energy absorption under dynamic loading

Specific Energy absorptions before densification of five foldcores are shown in Figure 13. Energy absorption (E) is calculated based on unit mass. Specific Energy absorption (SEA) is obtained by using the energy absorbed before densification of one unit cell dividing the mass of each unit cell, expressed with the following equations [37].

$$E = \int_0^{\delta_D} P(\delta) \cdot d\delta = A_{base} \cdot H\varepsilon_D \cdot \int_0^{\varepsilon_D} \sigma(\varepsilon) \cdot d\varepsilon = A_{base}H \cdot \sigma_{ave} \cdot \varepsilon_D;$$

$$SEA = \frac{E}{m} = \frac{E}{\rho \cdot V} = \frac{A_{base}H \cdot \varepsilon_D \cdot \sigma_{ave}}{\rho \cdot \rho_v \cdot A_{base}H} = \frac{\varepsilon_D \cdot \sigma_{ave}}{\rho \cdot \rho_v};$$

where P is the crushing force, A_{base} is the base area for each unit cell, H is the height of foldcore, δ is the crushing distance, δ_D is the crushing distance at densification, σ_{ave} is the average stress before densification, ε_D, is the densification strain, V is the volume of the material in the foldcore, ρ is the material density, ρ_v is the volumetric density of the foldcore, m is the mass of each unit cell.

As observed in Figure 13, energy absorption of cube strip is the mostly affected foldcore by crushing speed among these five structures. The energy absorption of cube strip increases by 184% from 2.51 to 7.13 J/g with the loading rate rising from 0.05 m/s to 25 m/s. D20-OT has the highest energy absorption capacity per unit mass under low speed crushing, around 3.46 J/g comparing with 2.51 J/g of cube strip foldcore. It also demonstrates an insensitive characteristic of energy absorption against different crushing velocities. Similar insensitivity can be found in another foldcore with open top, D10-OT. The closed top foldcores, D10-CT and D20-CT show a good performance under low crushing speed, the increase of crushing resistance under high loading rate leads to large increase in energy absorption.

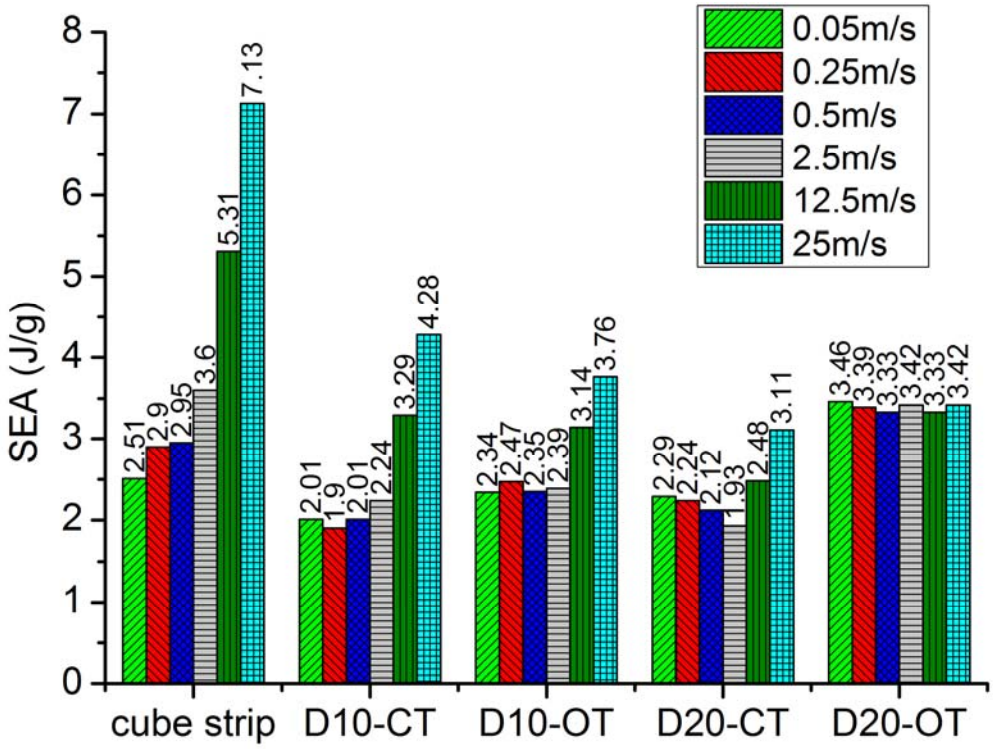

Figure 13. Specific energy absorption (SEA) before densification of five foldcores under various crushing speeds.

Increase in energy absorption of cube strip foldcore can be caused by the inertial effect of the structure and inertial stabilization of cell wall against buckling. Both initial peak stress and sequential folding stress rise with increasing in crushing velocity as shown in Figure 12 (a). For the square dome foldcores with closed top, i.e. D10-CT and D20-CT, their energy absorption capacities are more consistent with varying loading rate comparing with cube strip foldcore, although they are affected greatly only at high crushing speed. Extra constraints are added to the sidewalls for closed top foldcores because of the top face. The top face provides crushing resistance and stabilises the sidewalls under dynamic loading, which explains the sharp increase of initial peak stress. Under high loading rate, the buckling location of the sidewalls is shifted upwards, as shown in Figure 14. With the sidewall buckling location closer to the top face where extra inertia and stabilization effect provided by top face, the foldcore becomes stiffer to deform. As mentioned previously, inertial effects increase significantly at

high loading rate. Therefore, the closed top square dome foldcore D10-CT, D20-CT have a relatively consistent energy absorption capacity at low crushing speed, but a significant increase at high crushing speed.

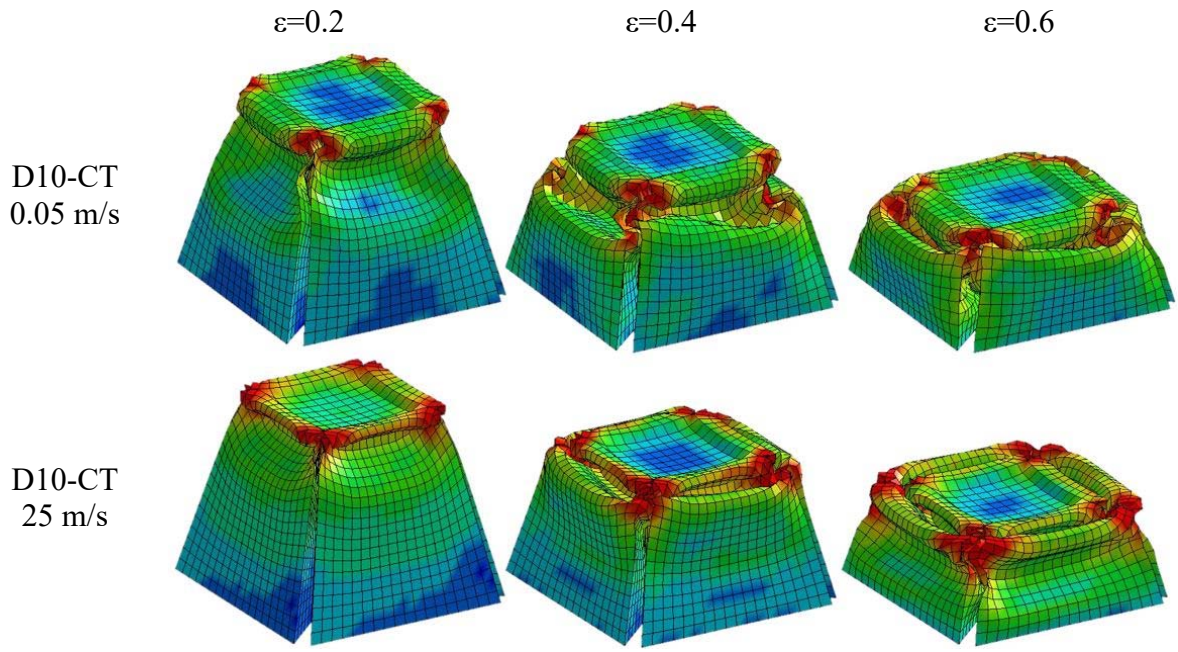

Figure 14. Damage modes of D10-CT at the strain of 0.2, 0.4 and 0.6 under the loading rates of 0.05 m/s and 25 m/s (Effective stress contour plot)

As for the square dome foldcores with open top, the stabilization effect of top square face no longer exists in dynamic crushing which leads to a more consistent energy absorption behaviour regardless of the loading rate. As explained previously, the top face provides resistance to the bending action of sidewalls at the top edges and it stabilizes sidewalls of unit cell under a higher crushing speed. D20-OT with a larger unit cell size and smaller interconnections than D10-OT, shows a more consistent energy absorption capacity with varying loading rates. Without the top face and less vertical resistance from interconnections, the damage mode of D20-OT at the early stage is not much affected by the increasing crushing rate from 0.05 m/s to 25 m/s, as shown in Figure 15. The damage modes of the foldcore at the strain of 0.2 show little change under different loading rates. The initiating location of buckling moves from corners to the centre of the sidewalls as shown in Figure 15 at the strain of 0.4 and

0.6 when the loading rate changes from 0.05 m/s to 25 m/s. The bending on top edge and overall buckling of sidewall, however, shows little difference between the two loading rates. Therefore, the reaction force remains similar in value, and there is little influence in energy absorption capacity for open-top square dome foldcore D20-OT under different loading rates.

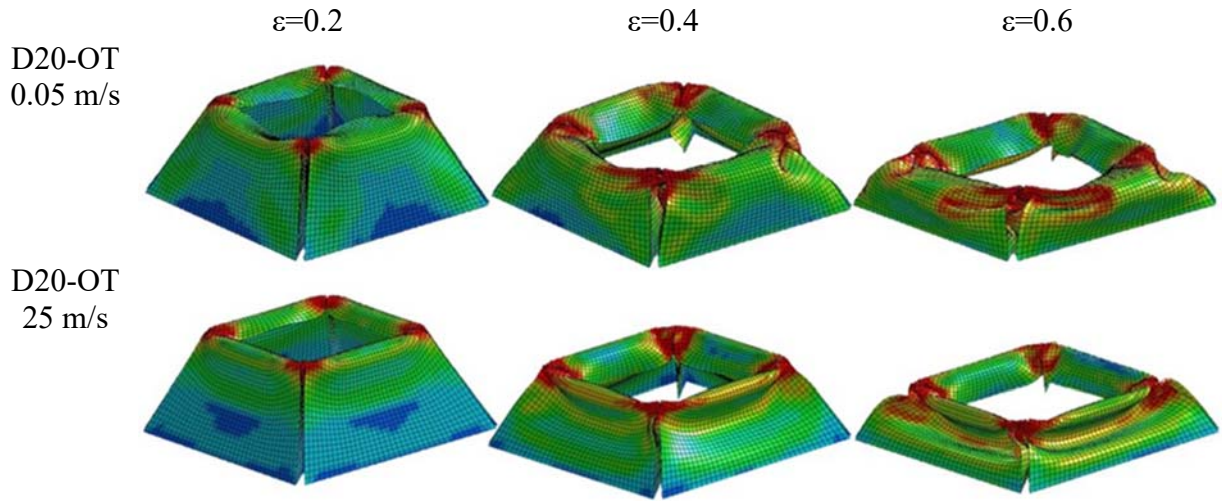

Figure 15. Damage modes of D20-OT at the strain of 0.2, 0.4 and 0.6 under the loading rates of 0.05 m/s and 25 m/s (Effective stress contour plot)

6. Conclusion

A new form of kirigami foldcore with square dome is proposed in this study. Unlike the existing top-performing kirigami foldcores, the proposed foldcore can be manufactured by using one whole patterned sheet instead of strips. Energy absorption capability is examined under both quasi-static and dynamic flatwise crushing. Good uniformity of collapsing of cell wall is demonstrated with low ratio of peak and average stress. The foldcore D20-OT outperforms the other three configurations of square dome foldcores and cube strip core by providing lower initial peak stress, higher plateau stress and energy absorption capability. Different crushing speeds are also applied onto these foldcores, and all the proposed square dome foldcores show less sensitivity of strain rate than cube strip core due to their unique geometries. The square dome foldcores experience different damage modes because of the top face, the inclining

sidewalls and the triangular interconnections. The square dome foldcore with open top outperforms the closed-top ones with the initial peak stress and energy absorption capacity less sensitive to strain rate. As the structure is proposed to be folded using one pre-cut sheet, the dimensions of the square dome are restrained. Given a set of base length and height, the inclining angle, interconnections geometries etc. are restrained in a set of value, unlike the cube strip kirigami foldcore where the height, width, length of unit cell can be any arbitrary number. The geometries such as inclining angle, core height and interconnection dimension can potentially affect the damage modes and energy absorption capacity, especially under dynamic loading conditions. Further study needs be conducted to define the optimized square dome foldcore geometries depending on the different applications as well as the potential application such as sacrificial cladding using folded square dome as core, due to its uniform crushing resistance and strain rate insensitivity.

7. Acknowledgements

The authors acknowledge the support from Australian Research Council via Discovery Early Career Researcher Award (DE160101116).

8. References

[1] G. Lu, T. Yu, Energy Absorption of Structures and Materials, Woodhead publishing limited, Cambridge England, 2003.

[2] M.F. Ashby, A. Evans, N.A. Fleck, L.J. Gibson, J.W. Hutchinson, H.N.G. Wadley, Metal foams: a design guide, Materials & Design, 23 (2002) 119.

[3] W. Hou, F. Zhu, G. Lu, D.-N. Fang, Ballistic impact experiments of metallic sandwich panels with aluminium foam core, Int. J. Impact Eng., 37 (2010) 1045-1055.

[4] Z. Xue, J.W. Hutchinson, Crush dynamics of square honeycomb sandwich cores, International Journal for Numerical Methods in Engineering, 65 (2006) 2221-2245.

[5] L.L. Hu, T.X. Yu, Dynamic crushing strength of hexagonal honeycombs, International Journal of Impact Engineering, 37 (2010) 467-474.

[6] F. Zhu, L. Zhao, G. Lu, Z. Wang, Deformation and failure of blast-loaded metallic sandwich panels—Experimental investigations, Int. J. Impact Eng., 35 (2008) 937-951.

[7] D.J. Sypeck, H.N.G. Wadley, Cellular Metal Truss Core Sandwich Structures, Advanced Engineering Materials, 4 (2002) 759-764.

[8] R.A.W. Mines, On the characterisation of foam and micro-lattice materials used in sandwich construction, Strain, 44 (2008) 71-83.

[9] G.J. McShane, D.D. Radford, V.S. Deshpande, N.A. Fleck, The response of clamped sandwich plates with lattice cores subjected to shock loading, European Journal of Mechanics - A/Solids, 25 (2006) 215-229.

[10] S. Hou, C. Shu, S. Zhao, T. Liu, X. Han, Q. Li, Experimental and numerical studies on multi-layered corrugated sandwich panels under crushing loading, Composite Structures, 126 (2015) 371-385.

[11] S. Li, Z. Wang, G. Wu, L. Zhao, X. Li, Dynamic response of sandwich spherical shell with graded metallic foam cores subjected to blast loading, Composites Part A: Applied Science and Manufacturing, 56 (2014) 262-271.

[12] S. Li, X. Li, Z. Wang, G. Wu, G. Lu, L. Zhao, Finite element analysis of sandwich panels with stepwise graded aluminum honeycomb cores under blast loading, Composites Part A: Applied Science and Manufacturing, 80 (2016) 1-12.

[13] W. Chen, H. Hao, Experimental investigations and numerical simulations of multi-arch double-layered panels under uniform impulsive loadings, Int. J. Impact Eng., 63 (2014) 140-157.

[14] W. Chen, H. Hao, Numerical simulations of stiffened multi-arch double-layered panels subjected to blast loading, International Journal of Protective Structures, 4 (2013) 163-188.

[15] W. Chen, H. Hao, Numerical study of a new multi-arch double-layered blast-resistance door panel, International Journal of Impact Engineering, 43 (2012) 16-28.

[16] G. Imbalzano, P. Tran, T.D. Ngo, P.V.S. Lee, A numerical study of auxetic composite panels under blast loadings, Compos. Struct., 135 (2016) 339-352.

[17] K.K. Saxena, R. Das, E.P. Calius, Three Decades of Auxetics Research − Materials with Negative Poisson's Ratio: A Review, Adv. Eng. Mater., (2016).

[18] S. Heimbs, P. Middendorf, S. Kilchert, A.F. Johnson, M. Maier, Experimental and Numerical Analysis of Composite Folded Sandwich Core Structures Under Compression, Applied Composite Materials, 14 (2008) 363-377.

[19] R.K. Fathers, J.M. Gattas, Z. You, Quasi-static crushing of eggbox, cube, and modified cube foldcore sandwich structures, International Journal of Mechanical Sciences, 101-102 (2015) 421-428.

[20] J.M. Gattas, Z. You, The behaviour of curved-crease foldcores under low-velocity impact loads, International Journal of Solids and Structures, 53 (2015) 80-91.

[21] K. Miura, Zeta-core sandwich-its concept and realization, title ISAS report/Institute of Space and Aeronautical Science, University of Tokyo, 37 (1972) 137.

[22] J.M. Gattas, Z. You, Miura-Base Rigid Origami: Parametrizations of Curved-Crease Geometries, Journal of Mechanical Design, 136 (2014) 121404-121404-121410.

[23] J.M. Gattas, W. Wu, Z. You, Miura-Base Rigid Origami: Parameterizations of First-Level Derivative and Piecewise Geometries, Journal of Mechanical Design, 135 (2013) 111011-111011-111011.

[24] J.M. Gattas, Z. You, Geometric assembly of rigid-foldable morphing sandwich structures, Eng. Struct., 94 (2015) 149-159.

[25] S. Heimbs, Foldcore sandwich structures and their impact behaviour: an overview, in: Dynamic failure of composite and sandwich structures, Springer, 2013, pp. 491-544.

[26] S. Liu, G. Lu, Y. Chen, Y.W. Leong, Deformation of the Miura-ori patterned sheet, International Journal of Mechanical Sciences, 99 (2015) 130-142.

[27] J.M. Gattas, Z. You, Quasi-static impact of indented foldcores, Int. J. Impact Eng., 73 (2014) 15-29.

[28] T. Nojima, K. Saito, Development of newly designed ultra-light core structures, JSME International Journal Series A Solid Mechanics and Material Engineering, 49 (2006) 38-42.

[29] A. Paul, U. Ramamurty, Strain rate sensitivity of a closed-cell aluminum foam, Materials Science and Engineering: A, 281 (2000) 1-7.

[30] T. Nieh, K. Higashi, J. Wadsworth, Effect of cell morphology on the compressive properties of open-cell aluminum foams, Materials Science and Engineering: A, 283 (2000) 105-110.

[31] E. Andrews, W. Sanders, L.J. Gibson, Compressive and tensile behaviour of aluminum foams, Materials Science and Engineering: A, 270 (1999) 113-124.

[32] B. Russell, V. Deshpande, H. Wadley, Quasistatic deformation and failure modes of composite square honeycombs, Journal of mechanics of materials and structures, 3 (2008) 1315-1340.

[33] W. Goldsmith, J.L. Sackman, An experimental study of energy absorption in impact on sandwich plates, International Journal of Impact Engineering, 12 (1992) 241-262.

[34] D. Ruan, G. Lu, F. Chen, E. Siores, Compressive behaviour of aluminium foams at low and medium strain rates, Composite Structures, 57 (2002) 331-336.

[35] F. Zhu, L. Zhao, G. Lu, E. Gad, A numerical simulation of the blast impact of square metallic sandwich panels, Int. J. Impact Eng., 36 (2009) 687-699.

[36] F. Côté, V.S. Deshpande, N.A. Fleck, A.G. Evans, The out-of-plane compressive behavior of metallic honeycombs, Materials Science and Engineering: A, 380 (2004) 272-280.

[37] N. Jones, Structural impact, Cambridge university press, 2011.